Physiologia Plantarum

ORIGINAL RESEARCH

Integrated Multivariate and Univariate Analysis of Circadian Metabolomic Signatures in Yerba Mate Clones in a Semi-Hydroponic System

Tamires O. Melo[1,2,3] | Joachim Kopka[2] | Ivar Wendling[3] | Alexander Erban[2] | Francisco A. Marques[1] | Fabricio A. Hansel[3]

[1]Departamento de Química, Universidade Federal do Paraná, Curitiba, Paraná, Brazil | [2]Max-Planck-Institut für Molekulare Pflanzenphysiologie, Potsdam-Golm, Germany | [3]Embrapa Florestas, Colombo, Paraná, Brazil

Correspondence: Fabricio A. Hansel (fabricio.hansel@embrapa.br)

Received: 18 February 2026 | **Accepted:** 15 April 2026

Handling Editor: M.A. Mutwil

ABSTRACT

This study presents an integrated multivariate and univariate analysis of circadian metabolomic signatures in *Ilex paraguariensis* (yerba mate) clones cultivated under semi-hydroponic conditions. Using repeated measures ANOVA–Simultaneous Component Analysis (RM-ASCA+) and hierarchical clustering on principal components (HCPC), we explored clone-specific and photoperiod-dependent metabolic responses across light and dark phases, complemented by high-resolution timepoint sampling (HRS) and targeted screening. Clone EC21 exhibited elevated levels of sugars, amino acids, and organic acids, suggesting a metabolic strategy adapted to saline stress and nocturnal energy demands. Photoperiod effects revealed circadian regulation of central carbon metabolites (e.g., glucose, fructose, maltose) and phenylpropanoid intermediates linked to bioactive compounds such as caffeoyl-quinic acids. Interaction effects highlighted metabolic plasticity, particularly in nitrogen assimilation, with compounds like 2-oxo-glutaric acid, glutamine, and ornithine showing clone-specific temporal patterns. Caffeine, a heritable and physiologically relevant metabolite, displayed distinct circadian profiles. EC24 accumulated caffeine during the day, while EC21 peaked at night. This dynamic distribution, supported by allantoin patterns in caffeine catabolism, suggests divergent nitrogen turnover strategies between clones. These findings underscore the importance of genotype selection and temporal regulation in optimizing yerba mate performance under semi-hydroponic systems. The combined use of RM-ASCA+ and univariate analysis proved to be a powerful approach for profiling metabolomic rhythms, offering valuable insights for breeding programs targeting bioactive compound enhancement, stress resilience, and metabolic efficiency.

1 | Introduction

Yerba mate (*Ilex paraguariensis* A. St. Hill.) is an arboreal species native to South American countries, including Brazil, Paraguay, Argentina, and Uruguay. It has been gaining popularity in global markets, with exports reaching more than 60 countries (Bracesco 2019). This increasing demand is largely due to the presence of phytochemicals in its leaves, which offer various health benefits, such as anti-inflammatory, anti-atherogenic, diuretic, and energizing effects (Heck and De Mejia 2007). Among the bioactive compounds found in yerba mate, caffeine (Ashihara et al. 2008) and phenolic compounds, such as chlorogenic acids (Palavicini et al. 2025), are particularly beneficial to human health. Yerba mate cultivation is carried out using native or planted trees (produced by seeds or by clones), under forest understory conditions, agroforestry systems, or monoculture

plantations in open fields (de Aguiar et al. 2023; Westphalen et al. 2020).

A semi-hydroponic system, already well-established for mini-cuttings production in yerba mate cloning, has been proposed for biomass and bioactive compounds production (Vieira et al. 2021; de Tomasi et al. 2024a, 2024b). Both biomass yield and bioactive compounds concentrations vary significantly across genotypes, highlighting the genotype-dependent nature of yerba mate (de Aguiar et al. 2022; de Tomasi et al. 2024b). One major advantage of this system is the ability to produce biomass every 20 days throughout the year, with frequent harvests of young and mature leaves. This contrasts with traditional field cultivation, where leaves and branches are harvested only once every 18–24 months (Santin et al. 2019).

For breeding programs aimed at producing bioactive compounds (e.g., caffeine) to be effective, high heritability of these compounds is required. Therefore, it is assumed that the expression of these compounds in plants is not (or is little) influenced by abiotic factors (e.g., light) (Dalmagro et al. 2018; Gutiérrez et al. 2008). However, the production and consumption of these bioactive compounds, and other metabolites, may naturally undergo biochemical changes to maintain basal biological activities necessary for plant growth and functioning, as well as in response to environmental variations (Richter et al. 2015; Mehta and Vyas 2023; Salam et al. 2023). This occurs because the metabolism and physiology of all organisms are natural processes that, when not altered by external agents, are endogenously generated and self-sustaining (Kiełbowicz-Matuk and Czarnecka 2014).

In the initial phase of the yerba mate breeding initiative, various clones exhibiting distinct phenotypes (i.e., biomass yield and caffeine levels) were chosen and cultivated in a semi-hydroponic system for the purpose of cloning, where their leaf biomass and caffeine contents were evaluated (Vieira et al. 2021). Concerns arise from the established plants in that semi-hydroponic environment about their ability to retain the phenotypic traits observed in the breeding program (i.e., biomass yield and bioactive compounds, de Aguiar et al. 2022; de Tomasi et al. 2024a). In this context, fundamental inquiries surface regarding the influence of circadian rhythms during yerba mate cultivation in a semi-hydroponic system. Circadian cycles incorporate temperature compensation mechanisms that prevent minor temperature fluctuations from causing significant variations in the biological clock (Gould et al. 2006; Dodd et al. 2005); this feature is feasible due to the inheritance of circadian rhythms, as originally proposed by Darwin (McClung 2006). Metabolites, which are the final products of various cellular activities, can be viewed as the connection between genotype and phenotype (Fiehn 2002). In plants, the circadian clock orchestrates metabolic processes to synchronize physiological activities with daily environmental cycles (Johnson 2005; Kuhlman et al. 2007). Rather than accelerating under temperature fluctuations, the circadian rhythm maintains near 24-h periodicity through temperature compensation mechanisms, although low temperatures can attenuate clock amplitude and modify metabolite accumulation patterns, as observed in *Arabidopsis thaliana* (Gould et al. 2006; Bieniawska et al. 2008; Dong and Farré Thomashow 2011).

During metabolome analysis, it is typical to examine several 100 analytes, making data interpretation a complex task. Therefore, integrating untargeted GC–MS multi-analyte data with multivariate analysis is crucial to uncover relationships among the dependent factors, for example, dark and light periods and clones (Paul and de Boves Harrington 2021). The incorporation of ANOVA—Simultaneous Component Analysis (ASCA) and its extensions, such as repeated measures ASCA+ (RM-ASCA+), offers a powerful framework for dissecting complex metabolomic data. By integrating general linear models with principal component analysis (PCA), these methods enable the decomposition and visualization of distinct experimental effects, even in unbalanced designs (Smilde et al. 2012; Thiel et al. 2017; Madssen et al. 2021). Applied to yerba mate clones, this approach may enhance the understanding of how circadian rhythms shape the metabolome responses across light and dark phases. Additionally, when high-dimensional data are involved (e.g., multiple time points across a day), Hierarchical Clustering on Principal Components (HCPC), which integrates PCA, hierarchical clustering, and proves useful for visualizing clusters through dendrograms and identifying quantitative variables significantly associated with these clusters (Husson et al. 2014). Following multivariate statistics, univariate statistical analysis can provide additional insights into how the circadian cycle significantly influences metabolites identified by the multivariate model (Melo et al. 2021; Menegolla et al. 2025). Considering the genotype-dependent nature of yerba mate with respect to both caffeine content (de Tomasi et al. 2024a) and biomass production (de Tomasi et al. 2024b), this methodology not only clarifies metabolic variations among clones but also helps the understanding of how circadian factors shape metabolite distribution. Such insights may inform breeding strategies aimed at enhancing bioactive compound levels and overall productivity in this species.

In summary, metabolome analysis can provide valuable insights into the interactions between genotype and environment in plants responding to different cultivation systems and environmental conditions. Yerba mate clones, which can be distinguished based on their genotypic differences, may exhibit changes in gene expression due to circadian regulation in semi-hydroponic systems. Therefore, metabolite profiling can help elucidate interactions between genotype and photoperiod, supporting breeding programs aimed at improving biomass production and the accumulation of heritable bioactive compounds in yerba mate. In this context, the present work aims to investigate the influence of the circadian cycle through untargeted metabolite analysis. Two clones with contrasting biomass production in the semi-hydroponic system were analyzed to explore genotype × photoperiod interactions.

2 | Material and Methods

2.1 | Plant Growth and Tissue Collection

The experiments were carried out at Embrapa Florestas located in Colombo (25.32° S, 49.16° W), using two experimental clones (EC24, EC21) from a breeding program (Sturion 2009) with distinct leaf biomass production (EC24–9.58 $kg\,m^{-2}\,year^{-1}$ and EC21–13.73 $kg\,m^{-2}\,year^{-1}$). The stock plants are far from

each other around 250 km (EC24—Quedas do Iguaçu (25.45° S, 52.91° W) and EC21—Barão de Cotegipe (27.62° S, 52.38°)). The plants used were cloned by the cutting technique in separate vessels. After 2 months, they were transplanted and kept in a mini clonal garden in a semi-hydroponic system with sand (Figure S1), allocated in a greenhouse, with periodic maintenance by pruning every 2.5 months. The plants were kept under drip irrigation with nutrient solution twice a day (2.5 L m^{-2}, Wendling et al. 2007) for a period of 4 min and 40 s. Plant material (i.e., mature leaves) for metabolome analysis was collected after 16 months, in the week before maintenance pruning. The circadian experiment was held, respecting the stimuli, bright, with collections before and after sunrise and sunset (Figure 1). According to Simepar (Paraná Meteorological System), on the collection date the temperatures had few fluctuations with a maximum temperature of 19°C registered at 14:00 h and minimum of 13°C at 5:00 h. Two radiation peaks were registered, one at 11:00 am and the other at 2:30 pm with the values of 2000 and 1800 μmol m^{-2} s^{-1}, respectively. The experiment involved 12 treatments (two clones across six time points), with 4 or 5 biological replicates, resulting in unbalanced data. For the targeted analysis, the data were reorganized to compare dark (ASS, MN, BSR) and light (ASR, MD, BSS) phases, which provided 13 or 14 replicates for each restructured treatment.

2.2 | Metabolite Analysis

The extraction and metabolite profiling were performed as previously described by (Dethloff et al. 2014), with slight modifications. Briefly, 20 mg (±5 mg) of fresh-frozen and ground plant material (i.e., mature leaves) were mixed with 300 μL of pre-cooled methanol in 2 mL microcentrifuge tubes. The solution was vortexed and supplemented with 30 μL of $^{13}C_6$-sorbitol (internal standard, 0.2 mg mL^{-1} in methanol) and 30 μL of *n*-nonadecanoic acid (extraction control, 2.0 mg mL^{-1} in chloroform). Extraction was carried out at 70°C and with agitation at 450 rpm for 15 min. After cooling to room temperature, 200 μL of chloroform were added, followed by vortexing and incubation in a thermomixer at 37°C and 450 rpm for 5 min. Subsequently, 400 μL of ultrapure water were added, the mixture was vortexed for 20 s, and centrifuged at 9659 *g* for 7 min. From the resulting biphasic solution, two aliquots (160 μL each) of the polar upper phase were transferred to separate 1.5 mL conical microcentrifuge tubes and dried under vacuum at room temperature. Methoximation was carried out by adding 40 μL of a solution containing 4-(dimethylamino) pyridine (5 mg mL^{-1}) and methoxyamine hydrochloride (40 mg mL^{-1}) in pyridine to the dried extracts. The mixture was incubated in a thermomixer at 30°C and 950 rpm for 90 min. Subsequently, trimethylsilylation was performed by adding 70 μL of N,O-bis(trimethylsilyl)trifluoracetamid (BSTFA) and 10 μL of a standard mixture of *n*-alkanes in pyridine (Dethloff et al. 2014), followed by vortexing and incubation at 37°C and 950 rpm for 30 min in a thermomixer. The samples were centrifuged at 20,817 *g* for 5 min, and an 80 μL aliquot of the supernatant was transferred to conical glass vials for GC–MS analysis.

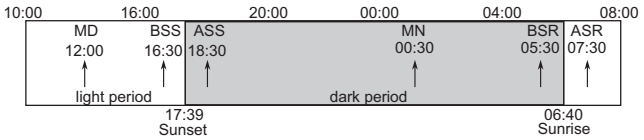

FIGURE 1 | Circadian sample collection strategy in yerba mate clones. Sampling was conducted at six time points: Midday (MD), before sunset (BSS), after sunset (ASS), midnight (MN), before sunrise (BSR), and after sunrise (ASR), under natural light conditions with 11 h of light and 13 h of darkness. Arrows indicate collection times aligned with light stimuli: Before (16:30 h and 5:30 h) and after (18:30 h and 7:30 h) sunrise and sunset.

Polar metabolite profiling was performed using a 6890 N24 gas chromatograph (Agilent Technologies) coupled to a Pegasus III TOF mass spectrometer (LECO Instrumente GmbH). Separation was achieved on a VF-5MS capillary column (30 m × 0.25 mm, 0.25 μm film thickness and an integrated 10 m guard-column) with splitless injection. The oven program consisted of an initial temperature of 70°C (1 min), followed by heating at 9°C min^{-1} up to 350°C (5 min). Injector temperature was set to 230°C, with helium carrier gas (0.6 mL min^{-1}). The GC–MS interface and ion source were both maintained at 250°C. The mass spectrometer operated in positive electron ionization mode (70 eV) with a mass range of 70–600 Da. Chromatograms were acquired, visually controlled, baseline corrected and exported in NetCDF file format using ChromaTOF (v. 4.22; LECO). Compounds were identified by mass spectral and RI matching to the reference collection of the Golm Metabolome Database (Hummel et al. 2010; Kopka et al. 2005) under manual supervision using TagFinder software (Luedemann et al. 2008). Guidelines for manually supervised metabolite identification were suggested by Strehmel et al. (2008). For relative abundance (a.u. g^{-1}), the intensities of the metabolites (i.e., peak height) were normalized by the fresh weight of the samples (g) and internal standard ($^{13}C_6$-Sorbitol). Annotated metabolites received an internal identification number, using the prefix "C" followed by running numbers, to support numerical data analyses (Table S1).

2.3 | Post-Analysis Treatment

Firstly, for data filtering, a percentage relative abundance based on total amount of annotated compounds (a.u. g^{-1}) was calculated, then a threshold of 0.01% was applied to the percentage relative abundance matrix, and compounds below this limit were considered non-detected. Secondly and independently in the annotated normalized matrix (i.e., fresh weight of the samples and internal standard, see above) all compound amount values (a.u. g^{-1}) identified previously (including missing ones, attributed as zero) were used to calculate the minimum detectable amount according to Skoog et al. (1996). The calculated value (a.u. g^{-1}) was used to replace the corresponding entries in the dataset.

Univariate statistical analyses were conducted in R (R CoreTeam 2018) using the packages *stats*, *multcomp*, *lattice*, *agricolae*, and *effects*. Prior to model selection, metabolite data were evaluated for normality and homoscedasticity. Based on the fulfillment of these assumptions, the appropriate statistical approach was applied, including analysis of variance (ANOVA), generalized linear models (GLM), or non-parametric tests. Post hoc comparisons among treatments were performed with

adjustment for multiple testing, adopting a significance threshold of $p < 0.05$, with Tukey's Honestly Significant Difference (HSD) test used following ANOVA, single-step adjustment applied for GLM, and the Holm correction employed for non-parametric analyses (Melo et al. 2021).

The multivariate analyses employed in this study included repeated measures—ANOVA Simultaneous Component Analysis (RM-ASCA+), Principal Component Analysis (PCA), and Hierarchical Clustering on Principal Components (HCPC), each selected for its ability to explore and visualize metabolite distribution patterns across experimental conditions. RM-ASCA+ was used to decompose the variability associated with different factors and their interactions, and HCPC was particularly valuable for detecting structure within high-dimensional time series data, enabling the identification of distinct metabolite clusters and their association with specific experimental phases. All multivariate analyses were performed using R software, utilizing packages such as ALASCA (RM-ASCA+), factoMineR, and factoextra (Husson et al. 2014; Jarmund et al. 2022; R CoreTeam 2018).

3 | Results

3.1 | General Aspects of Circadian High-Resolution Time-Point Sampling Strategy (HRS)

Metabolite profiling of yerba mate clone leaves across the circadian cycle resulted in the detection of 148 metabolites, of which 74 signals were annotated, corresponding to 52% of the total detected features. The predominant chemical classes comprised amino acids, phenolic compounds, sugars, organic acids, sugar acids, nitrogen-containing compounds, and sugar alcohols. Carbohydrates and their derivatives (including sugar acids and sugar alcohols) accounted for a substantial proportion of the extract, with sucrose being the most abundant compound. Notably, a large fraction of the unidentified metabolites exhibited characteristic carbohydrate-associated mass fragments (m/z 217, 205, and 319), suggesting their structural relation to carbohydrate derivatives. Central carbohydrate metabolism was represented by key intermediates such as glucose-6-phosphate, fructose-6-phosphate, glucose, fructose, sucrose, and maltose. Organic acids were predominantly associated with the tricarboxylic acid (TCA) cycle, including succinic, 2-oxoglutaric, fumaric, citric, and malic acids. Nitrogen metabolism was characterized by the presence of amino acids such as glutamic acid, aspartic acid, glutamine, and asparagine. Additionally, characteristic bioactive metabolites of yerba mate with recognized health-promoting properties, including caffeine and chlorogenic acids, were also identified (Table S1).

First, PCA were employed to reveal the underlying structure of the data using semi-quantitative data of known and unknown metabolites (Figure S2). In the circadian cycle, the first six principal components (PC) encompassed 77.2% of the total variance from this data set; such a high number of PCs was necessary to explain the complexity of a high-dimensional dataset. The huge dataset involved 2 yerba mate clones and 6 sampling times (i.e., 54 individuals including their replicas), which are described by 148 variables. Thus, these numbers of PCs (i.e., 6 for circadian cycle) were used as a pre-processing step for the clustering (Husson et al. 2014). Thus, the hierarchical clustering dendrogram serves as a summary of the distance matrix, which reveals the similarities and differences between individuals in each cluster. Dendrograms of hierarchical clustering based on Ward's criterion with a graph output of inertia gain is shown in Figure 2.

In the circadian cycle, 12 clusters were depicted summing sampling time and clones; this number of optimal clusters was estimated by the ratio of two successive within-group inertia that gives the small possible value (WI), in this case $0.388 = 3.956/10.195$, and by the visualization of inertia gain, in which any decrease is seen after 12 clusters (Figure 2, insert). Based on the hierarchical clustering, three major clusters are observed, considering that the height of the branches indicates the dissimilarity between the clusters. The first group has samples ASS for clone EC24 and BSS for clone EC21; both samples were collected around sunset, before and after sunset for clones EC21 and EC24, respectively. The second with sampling times MN, ASR, MD, and ASS for clone EC21, and the third has the rest

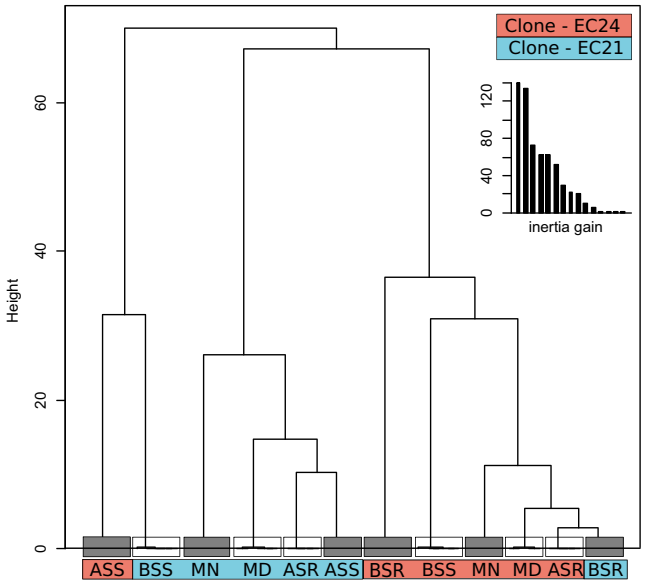

FIGURE 2 | Hierarchical Clustering on Principal Components (HCPC) based on Ward's criterion, applied after $\log_2$ data transformation. The height of dendrogram branches represents the dissimilarity between clusters. Cluster assignment was determined from sample coordinates projected onto the first six principal components. Abbreviations: EC24 and EC21 (Clones), midday (MD), before sunset (BSS), after sunset (ASS), midnight (MN), before sunrise (BSR), and after sunrise (ASR). Inset: Inertia gain plot illustrating the evolution of within-group inertia during agglomeration. Ward's criterion, derived from the Huygens theorem, decomposes the total inertia into between- and within-group variance. At each step, clusters are merged to minimize the increase in within-group inertia, and the optimal number of clusters is generally inferred from both the dendrogram structure and the inertia gain plot (Husson et al. 2010). In this case, 12 clusters were identified. Principal components beyond PC6 (up to PC10, explaining 93.7% of variance) were examined, but did not reveal additional biological structure, suggesting that residual variance reflects background noise rather than meaningful signal.

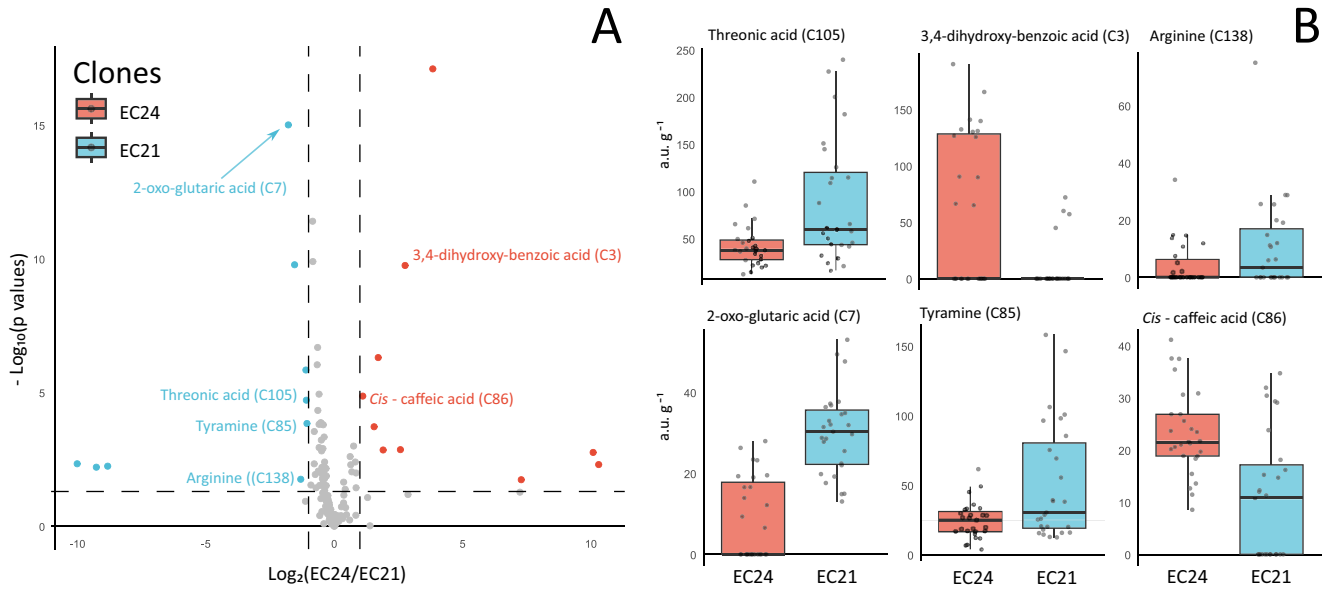

FIGURE 3 | Univariate statistical volcano plot illustrating the clone effect (EC21 vs. EC24, $n = 27$). Log_2 fold change (FC) represents the ratio of the mean values (a.u. g^{-1}) of each metabolite. Each dot corresponds to a single metabolite: Gray dots indicate non-significant differences (FC < 1.0 and $p > 0.05$), blue dots represent metabolites significantly more abundant in clone EC21 ($p < 0.05$), and red dots represent metabolites significantly more abundant in clone EC24 ($p < 0.05$) (A). Box plots display the mean values (a.u. $g^{-1} \pm$ SE, $n = 27$) of the metabolites highlighted in the volcano plot (B).

of the sampling times for clone EC24, and one sample of clone EC21 (BSR). Most samples are grouped considering the clone factor, so it seems that clone factors are more important than sampling times, even with respect to the dark and light periods.

Although clustering analysis distinguished the effects of clone variation across the circadian cycle, a large number of metabolites were required to resolve this complex system. Interestingly, several unannotated metabolites also contributed substantially to the observed separations. To identify the most significant annotated compounds differentiating the clones, a volcano plot was generated comparing EC24 and EC21 using cutoffs of $p \leq 0.05$ and $\log_2$ fold change ≥ 1 (Figure 3A). Only six annotated metabolites showed significant contributions across the circadian cycle. These compounds are associated with physiological balance and leaf tissue resilience to environmental stress. Specifically, *cis*-caffeic acid (C86) and 3,4-dihydroxybenzoic acid (C3) were more abundant in clone EC24, while tyramine (C85), threonic acid (C105), 2-oxo-glutaric acid (C9), and arginine (C138) were enriched in clone EC21 (Figure 3B).

3.2 | Contrasting the Dark and Light Periods

To streamline metabolomic analysis and prioritize biologically interpretable outcomes, we transitioned from high-resolution sampling (HRS), which involved six time-point collections per day, to a more targeted approach focused exclusively on annotated metabolites. The data were reorganized to contrast dark (ASS, MN, BSR) and light (ASR, MD, BSS) phases. However, following this adjustment, PCA and HCPC failed to effectively separate the experimental groups (Figures S3 and S4). As a result, we applied RM-ASCA+, which enables direct evaluation of clone effects, photoperiod influence, and their interactions on metabolite profile shifts. By restricting the analysis to identified compounds, we enhanced biological relevance and reduced model complexity, facilitating clearer insights into circadian-driven metabolomic variation across light and dark periods.

The RM-ASCA+ analysis revealed a clear partitioning of variance across three principal components, each providing distinct insights into the metabolomic dynamics of yerba mate clones (Figure 4). PC1, which explained the largest proportion of variance (52.2%), was strongly associated with the clone effect, highlighting systemic shifts in metabolite profiles between clones EC24 and EC21 (Figure 4A), consistent with patterns observed in the previous HCPC analysis (Figure 2). PC2, accounting for 28.2% of the variance, captured the photoperiod effect, distinguishing metabolic profiles between the dark (MN, BSR, ASS) and light (MD, BSS, ASR) phases (Figure 4B). Meanwhile, PC3, contributing 19.6% of the variance, reflected the interaction between clone and photoperiod, reflecting differential metabolic plasticity among genotypes in response to circadian modulation (Figure 4C).

All annotated metabolites (74 variables) underwent univariate statistical analysis, being 46 compounds statistically significant (Tables 1–3). Most of the univariate results were in strong concordance with the key metabolites in RM-ASCA+ findings (Figure 4D–F). These metabolites included amino acids, organic acids (notably TCA cycle intermediates), sugars, and their derivatives, such as acids, alcohols, and phosphates. Sugar distribution was particularly significant in clone separation: 15 compounds contributed to this effect, with clone EC21 showing higher sugar content, except for mannose (C124) (Table 1). Eight sugars were associated with photoperiod, with elevated levels observed during the dark phase, highlighting the sugars of central carbohydrate metabolism glucose (C121), fructose (C118), and maltose (C123, Table 2). Regarding the interaction factor, only fucose (C119) showed statistical significance.

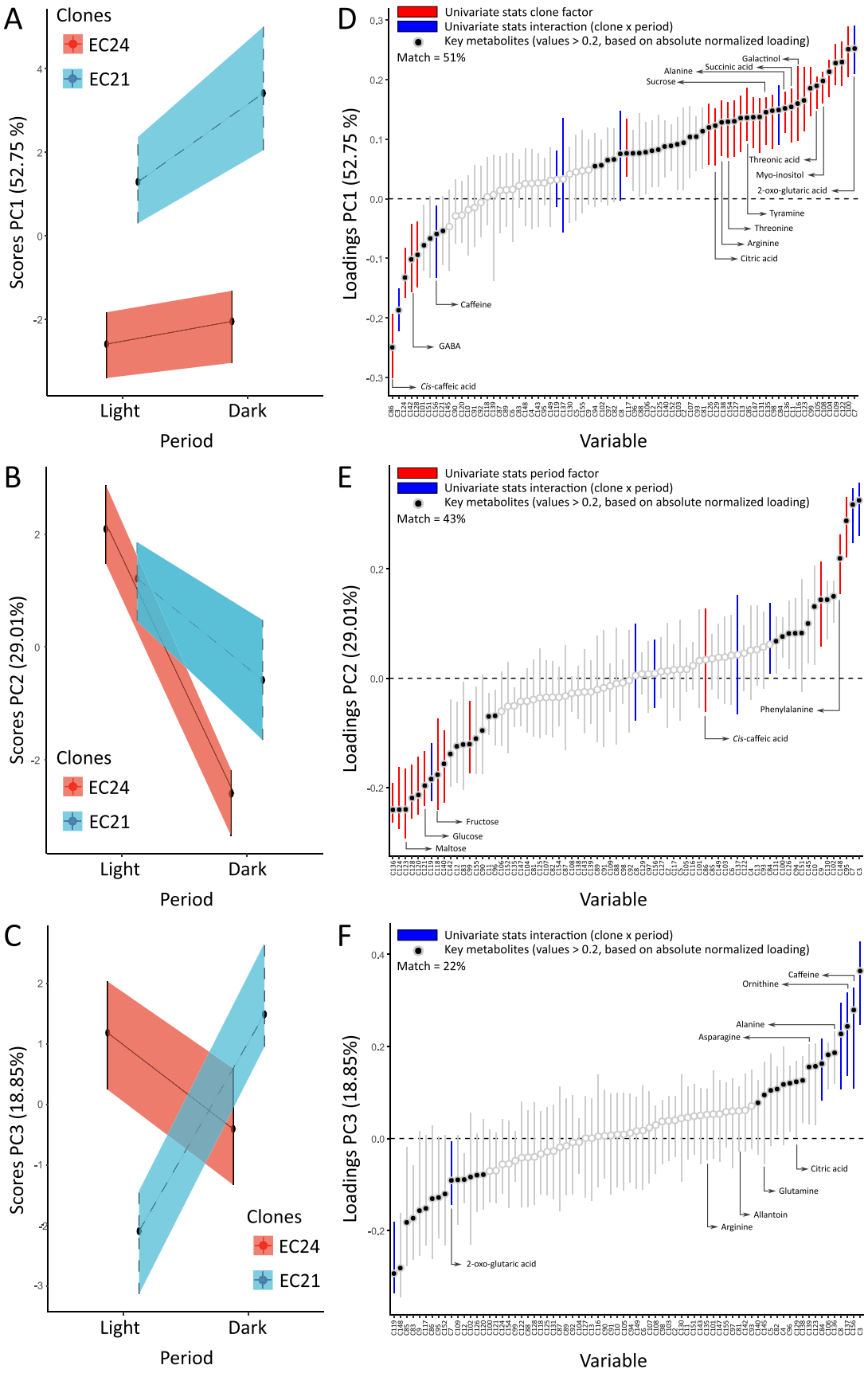

FIGURE 4 | Legend on next page.

FIGURE 4 | Results from Repeated Measures ANOVA–Simultaneous Component Analysis plus Linear Mixed Models (RM-ASCA+) showing metabolomic variation associated with clone, photoperiod (dark/light), and their interaction. The analysis was performed using the ALASCA package with default parameters, except for validate = True and wide = True (i.e., each observation occupies a separate row, with variables in separate columns; Jarmund et al. 2022). Score plots illustrate separation along principal components: PC1 distinguishes clones (EC24 in red, EC21 in blue) (A), PC2 separates photoperiods (B), and PC3 captures the interaction effect (C). Loading plots for PC1 (D), PC2 (E), and PC3 (F) highlight metabolites contributing to each effect, with a vertical dotted line separating high and low loadings. Each dot represents a metabolite: Gray dots indicate non-representative metabolites (absolute normalized loading [ANL] < 0.2), while black dots denote representative metabolites (ANL > 0.2). Dark red bars in plots D and E indicate metabolites also identified as significant in univariate analysis for clone (Table 1, $p < 0.05$) and photoperiod (Table 2, $p < 0.05$), respectively. Dark blue bars in plots D, E, and F mark metabolites showing significant interaction effects in univariate analysis (Table 3, $p < 0.05$). Match values represent the percentage overlap between metabolites with ANL > 0.2 (black dots) and those identified via univariate analysis (color bars). Error bars in both score and loading plots reflect 95% confidence intervals based on 1000 bootstrap iterations. For metabolite codes in D, E and F see Table S1.

TABLE 1 | Mean values of statistically significant metabolites (a.u. $g^{-1} \pm$ SE, $n = 30$, $p < 0.05$) showing aclone effect based on univariate analysis of the photoperiod (dark vs. light) by a metabolite-targeted approach.

Code	Compounds	Classes	EC24	EC21
C136	Alanine	amino acid	41.7 ± 5.6	55.3 ± 7.3
C138	Arginine	amino acid	4.3 ± 1.5	10.7 ± 3.2
C142	4-amino-butanoic acid (GABA)	amino acid	80.0 ± 14.0	45.3 ± 5.0
C147	Glycine	amino acid	95.3 ± 8.1	127.1 ± 13.9
C154	Threonine	amino acid	124.8 ± 10.7	168.6 ± 15.2
C85	Tyramine	nitrogen compound	24.6 ± 2.6	51.3 ± 8.2
C11	Succinic acid	organic acid	84.4 ± 8.1	118.4 ± 11.5
C129	Citric acid	organic acid	36.7 ± 3.2	54.4 ± 9.3
C131	Quinic acid	organic acid	235.6 ± 14.5	309.3 ± 23.4
C13	Kampeferol	phenol	55.4 ± 3.2	74.3 ± 6.8
C86	Cis-caffeic acid	phenol	23.3 ± 1.6	10.8 ± 2.4
C98	Erythronic acid	sugar	69.4 ± 5.1	92.0 ± 7.4
C99	Galactaric acid	sugar	41.7 ± 3.4	59.2 ± 4.3
C100	Galactonic acid	sugar	61.3 ± 3.7	109.1 ± 7.1
C104	Saccharic acid	sugar	44.7 ± 2.7	67.4 ± 5.0
C105	Threonic acid	sugar	41.9 ± 4.2	89.0 ± 12.4
C108	Myo-inositol	sugar	128.3 ± 7.6	182.3 ± 13.2
C109	Ribitol	sugar	24.8 ± 1.8	39.2 ± 2.4
C116	Galactinol	sugar	42.8 ± 2.7	60.2 ± 5.2
C117	Arabinose	sugar	20.2 ± 2.3	33.1 ± 6.9
C122	1,6-anhydro-beta-glucose	sugar	64.7 ± 3.6	101.3 ± 6.4
C124	Mannose	sugar	65.6 ± 6.4	42.7 ± 5.0
C126	Ribose	sugar	109.5 ± 10.5	147.0 ± 10.1
C127	Ribulose	sugar	56.1 ± 5.1	77.4 ± 7.6
C128	Xylose	sugar	118.9 ± 8.9	92.2 ± 8.5
C135	Sucrose	sugar	289.8 ± 20.4	376.4 ± 33.2

TABLE 2 | Mean values of statistically significant metabolites (a.u. g^{-1} ± SE, $n = 30$, $p < 0.05$) showing photoperiod effect (dark vs. light) based on univariate analysis.

Code	Compounds	Classes	Light	Dark
C136	Alanine	amino acid	28.9 ± 2.2	68.1 ± 7.3
C140	Aspartic acid	amino acid	70.2 ± 5.7	97.4 ± 8.4
C148	Phenylalanine	amino acid	72.3 ± 6.9	33.6 ± 6.5
C9	Oxalic acid	organic acid	31.9 ± 4.0	21.2 ± 3.2
C86	Cis-caffeic acid	phenol	20.2 ± 2.1	13.8 ± 2.4
C95	Glyceric acid-3-phosphate	sugar	60.0 ± 6.9	21.2 ± 5.9
C99	Galactaric acid	sugar	45.0 ± 3.5	55.9 ± 4.6
C118	Fructose	sugar	19.5 ± 2.5	31.4 ± 5.2
C120	Galactose	sugar	62.0 ± 5.9	87.0 ± 8.8
C121	Glucose	sugar	282.1 ± 25.7	383.2 ± 43.0
C123	Maltose	sugar	42.2 ± 4.7	93.6 ± 9.1
C124	Mannose	sugar	44.6 ± 4.0	63.6 ± 7.3
C128	Xylose	sugar	91.1 ± 6.1	120.0 ± 10.6

TABLE 3 | Mean values of statistically significant metabolites (a.u. g^{-1} ± SE, $n = 15$, $p < 0.05$) showing interaction effects between clone and photoperiod (dark vs. light) based on univariate analysis.

Code	Compounds	Classes	EC24_light	EC21_light	EC24_dark	EC21_dark
C137	Ornithine	amino acid	14.6 ± 3.5	4.8 ± 2.3	6.7 ± 3.0	16.8 ± 5.1
C84	2-hydoxy-pyridine	nitrogen compound	25.5 ± 2.8	25.6 ± 1.6	19.0 ± 2.6	36.6 ± 5.9
C156	Caffeine	nitrogen compound	40.8 ± 4.1	20.6 ± 4.0	31.8 ± 3.0	35.7 ± 6.3
C7	2-oxoglutaric acid	organic acid	18.0 ± 1.8	32.7 ± 3.3	0.0 ± 0.0	27.2 ± 2.0
C8	Lactic acid	organic acid	20.2 ± 4.1	14.6 ± 1.7	16.0 ± 3.2	26.4 ± 3.3
C3	3,4-dihydroxy-benzoic acid	phenol	122.6 ± 10.1	0.0 ± 0.0	0.0 ± 0.0	18.1 ± 8.0
C119	Fucose	sugar	64.1 ± 6.3	88.2 ± 8.8	97.5 ± 9.3	83.2 ± 8.1

Seven amino acids were important for the main effects. Alanine (C135) was associated with both clone and photoperiod, while arginine (C138), GABA (C142), glycine (C147), and threonine (C154) were linked to clone differences, with GABA being the only one more abundant in EC24 (Table 1). Alanine (C136), aspartic acid (C140), and phenylalanine (C148) were associated with photoperiod, with phenylalanine accumulating during the light phase (Table 2). Ornithine (C137) was the only amino acid significantly affected by the interaction factor. Nitrogen compounds, 2-hydroxy-pyridine (C84), and caffeine (C156) showed strong relevance for the interaction factor (Table 3). Tyramine was more abundant in EC21, reflecting a clone-specific effect. Among organic acids, succinic acid (C11), citric acid (C129), and quinic acid (C131) were more abundant in EC21, indicating a clone effect. Oxalic acid (C9) was associated with the light photoperiod (Table 2), while 2-oxo-glutaric acid (C7) and lactic acid (C8) were significant for the interaction factor (Table 3). Only three phenolic compounds showed significant differences: kaempferol (C13) and *cis*-caffeic acid (C86) were linked to clone effects, with kaempferol more abundant in EC21 and *cis*-caffeic acid (C86) in EC24 (Table 1). *Cis*-caffeic acid (C86) also varied with photoperiod, accumulating during the light phase (Table 2). 3,4-Dihydroxy- benzoic acid (C3) was the only phenol showing a significant interaction between clone and photoperiod (Table 3).

Interestingly, the strong concordance between RM-ASCA+ and univariate statistical analyses reinforces the reliability of the identified metabolic markers (Figure 4D–F). When considering only RM-ASCA+ key metabolites with absolute normalized loading values above 0.2%, 51% of those associated with the clone effect were also identified in the univariate analysis. For the photoperiod effect, 43% of the metabolites overlapped, while 22% of those linked to the interaction factor were congruent between both approaches.

4 | Discussion

4.1 | Multivariate and Univariate Statistics Approaches

Initially, the circadian high-resolution time-point sampling strategy (HRS) was evaluated using Hierarchical Clustering on Principal Components (HCPC), which was preferred over traditional hierarchical cluster analysis (HCA), performing hierarchical clustering (HCA) directly on the original high-dimensional data can be problematic, as the large number of variables may introduce noise and reduce the interpretability of the clustering results. HCPC integrates dimension reduction through principal component analysis (PCA), extracting continuous variables that capture the most significant variance. These PCA results are then subjected to clustering, serving as a noise-filtering step to enhance robustness (Lê et al. 2008), with the advantage of exploiting a mixed algorithm for the clustering process, a combination of the Ward's classification method with the K-means algorithm (Maugeri et al. 2021).

While HCPC revealed a clear clone effect (Figure 2), the complexity of the data made it difficult to pinpoint which variables were driving the separation mainly due to a high number of unknown annotated compounds. To improve interpretability and maximize contrast between experimental factors (i.e., clone and photoperiod), the sampling strategy was refined from six time points per day to a more targeted design (dark vs. light periods). However, after this adjustment, HCPC failed to separate the groups effectively (Figures S3 and S4). This limitation likely stems from the unsupervised nature of HCPC, suggesting that clone and photoperiod differences do not represent the dominant source of variance in the dataset (Jolliffe 2002).

To address this, we incorporated external knowledge of the experimental design using RM-ASCA+, a supervised method that focuses not on total variance, but on the variance explained by predefined factors (Bertinetto et al. 2020), namely clone, photoperiod, and their interaction. The RM-ASCA+ model successfully isolated these targeted effects, confirming that both clone and photoperiod exert statistically significant influences on the metabolite profiles (Figure 4). To a certain degree, the concordance between RM-ASCA+ and univariate statistical analysis stems from their shared principle: both methods isolate and quantify the effect of one factor while controlling for others (Bertinetto et al. 2020), (Figure 4D–F). Results showed strong overlap between RM-ASCA+ and univariate analysis for the independent effects of clone and photoperiod, 51% and 43%, respectively (Figure 4D,E, Tables 1 and 2), while the interaction effect revealed a lower degree of overlap, 22% (Figure 4F, Table 3).

This indicates a more complex, multivariate phenomenon during interaction, where the metabolic shift is not driven by individual metabolites alone, but by a coordinated and subtle reorganization of the entire metabolome, captured through multivariate approaches. In this context, interaction was not driven predominantly at the level of single metabolites, and the evidence supports the view that the interaction reflects a distributed pattern involving multiple metabolites whose combined behavior differentiates clones across photoperiods. Finally, for selected metabolites, univariate analysis was applied to the HRS dataset to evaluate their rhythmic behavior across the six time points of the circadian cycle (Figure 5).

4.2 | Metabolic Inferred Saline Stress Environment

Clone main effect analysis revealed distinct metabolic profiles between yerba mate genotypes, with clone EC21 generally exhibiting higher amounts of sugars, amino acids, and organic acids (Figure 4, Table 1). Notably, several sugars abundant in EC21, such as sucrose (C135), galactinol (C116), *myo*-inositol (C108), threonic acid (105) (also detected in the HRS, Figure 3), and galactaric acid (C99), have been previously associated with salt stress responses in other plant species (Richter et al. 2015; Filippou et al. 2021), suggesting a potential role in osmotic adjustment and stress signaling. Similarly, organic acids like citric acid (C129), succinic acid (C11), also elevated in EC21, are TCA cycle intermediates known to contribute to redox balance and energy metabolism (Richter et al. 2015), potentially supporting EC21's energetic advantage under semi-hydroponic conditions.

Among amino acids, alanine (C136) and threonine (C154) were more abundant in EC21 and have been linked to osmotic regulation under stress (Filippou et al. 2021; Gavaghan et al. 2011), while GABA (C142), another stress-responsive metabolite (Ghosh et al. 2021; Patel et al. 2020), showed higher levels in EC24. Interestingly, EC24 also displayed elevated amounts of *cis*-caffeic acid (C86), a known antioxidant involved in scavenging reactive oxygen species (ROS) under salt stress (Mehmood et al. 2021). Tyramine (C85), arginine (C138), and 2-oxo-glutaric acid (C7) were also significant to the clone effect in the HRS (Figure 3), although only the TCA-related organic acid showed a known association with salt stress (Richter et al. 2015). During the dark/light photoperiod analysis, this compound followed an interaction pattern, further suggesting its plasticity between clones and photoperiod.

Soluble carbohydrates such as galactinol (C116), *myo*-inositol (C108), and sucrose (C135), found in higher amounts in clone EC21, are directly or indirectly linked to the raffinose family of oligosaccharides (RFOs). *Myo*-inositol plays a role in abiotic stress responses in plants (Ishitani et al. 1996; Valluru and Van den Ende 2011), and RFOs metabolites are known to accumulate under salt stress, functioning as osmoprotectants (Sengupta et al. 2015). Although organic acids from the TCA cycle typically decrease under high salinity conditions, possibly due to the metabolic shift toward osmoprotectant synthesis (Gavaghan et al. 2011; Takabe 2012), the elevated levels of citric and succinic acids in EC21 suggest enhanced energy metabolism, potentially supporting its growth under semi-hydroponic conditions. Indeed, biomass production in clone EC21 is superior to that of EC24 in this system (Vieira et al. 2021). These findings suggest that the clones may adopt distinct metabolic strategies; EC21 appears to favor the accumulation of osmolytes and energy intermediates, while EC24 shows increased levels of phenolic compounds and GABA, suggesting a stress response pathway centered on antioxidant and GABA shunt signaling functions, which allows the cell to recycle carbon and nitrogen under stress (Michaeli and Fromm 2015; Mehta and Vyas 2023).

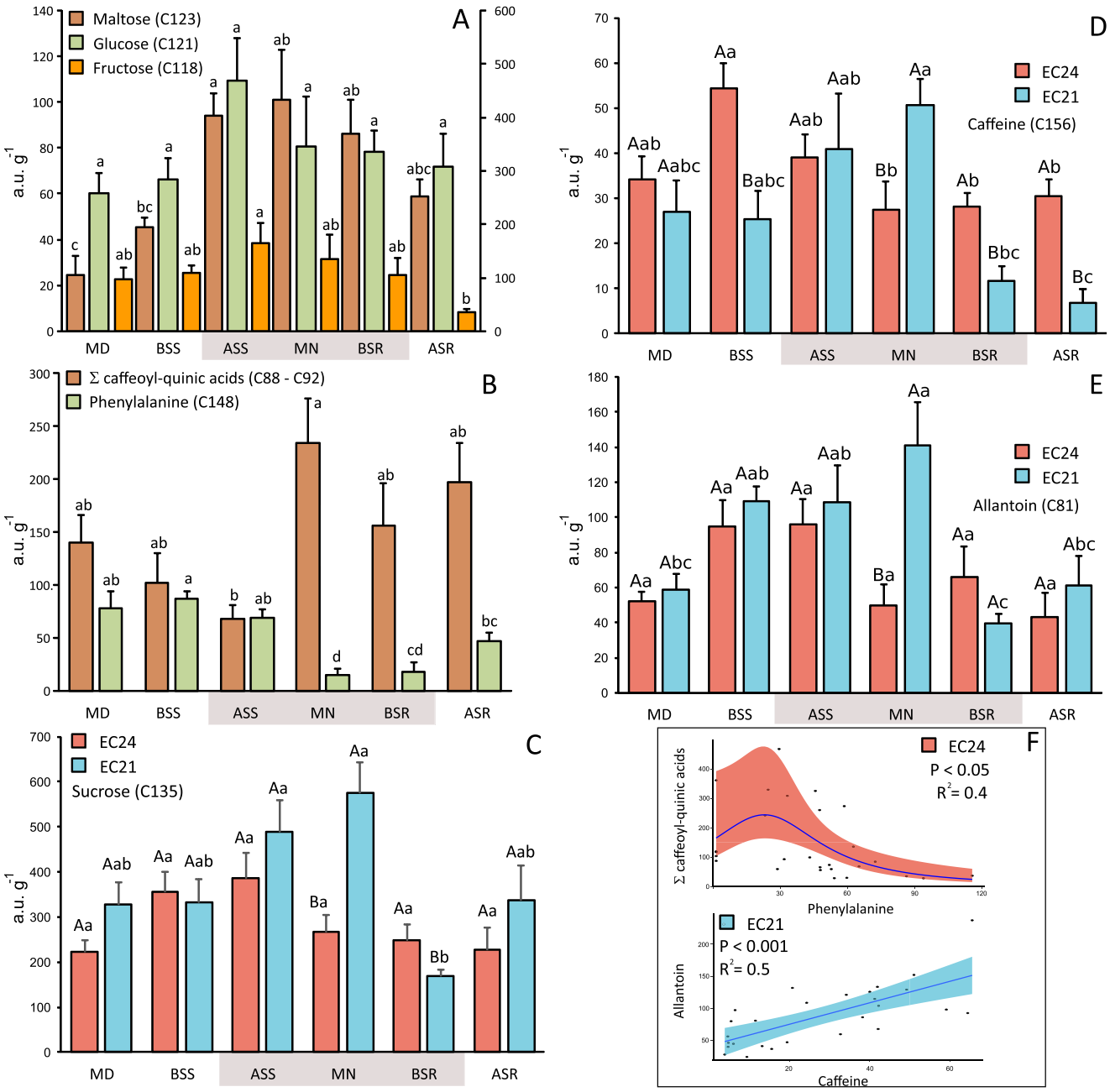

FIGURE 5 | Histograms of high-resolution time-point sampling for metabolites associated with photoperiod effects (A and B), interaction effects (C, D, and E), and regression curves for sum of caffeoyl-quinic acids versus phenylalanine and allantoin versus caffeine (F). Panel A shows maltose and fructose (left y-axis) and glucose (right y-axis); panel B shows the sum of caffeoyl-quinic acids and phenylalanine. Mean values (a.u. $g^{-1} \pm SE$, $n = 8–10$) followed by the same letter do not differ statistically across time-point sampling ($p < 0.05$). Panels C, D, and E show sucrose, caffeine, and allantoin, respectively, with mean values (a.u. $g^{-1} \pm SE$, $n = 4–5$). Capital letters indicate significant differences between clones (EC24 vs. EC21), while lowercase letters denote differences across time points within each clone ($p < 0.05$). Panel F presents regression curves (solid lines) and data points (dots, a.u. g^{-1}) for selected compounds, with shaded areas representing 95% confidence intervals. In all histograms, the dark periods are indicated by a grey box. Abbreviations: Midday (MD), before sunset (BSS), after sunset (ASS), midnight (MN), before sunrise (BSR), and after sunrise (ASR).

Semi-hydroponic systems represent a promising strategy for yerba mate biomass production, supporting both mature and young leaf development through soil-free cultivation and controlled nutrient delivery (de Aguiar et al. 2022; de Tomasi et al. 2024b). However, a key limitation of this approach may be its susceptibility to saline stress, which can result from nutrient accumulation over time. Elevated salinity disrupts osmotic balance, impairs root function, and reduces photosynthetic efficiency, ultimately constraining biomass yield (Hualpa-Ramirez et al. 2024). To ensure sustained productivity and system viability, it is essential to manage salt build-up through periodic flushing, customized nutrient formulations, and the selection of salt-tolerant (halophytic) genotypes.

Although yerba mate is not traditionally recognized as a halophytic species, emerging experimental data suggest that certain clones may possess some degree of resilience to saline conditions (de Aguiar et al. 2023). These indications, however, remain

preliminary, and targeted studies on stress tolerance in yerba mate are still limited (Gabira et al. 2024). In the context of semi-hydroponic systems, where nutrient accumulation can intensify salinity stress, the selection of salt-tolerant genotypes becomes especially critical. This approach has proven effective in other crops, where identifying and cultivating halophytic varieties has significantly improved system performance and biomass yield (Hualpa-Ramirez et al. 2024).

Additionally, metabolomic profiling offers a powerful tool to advance our understanding of yerba mate's physiological responses to the potential salinity environment (Jorge et al. 2017). By analyzing shifts in metabolic pathways under semi-hydroponic conditions, both multivariate (e.g., RM-ASCA+) and univariate analyses can help identify biomarkers of tolerance and guide the selection of genotypes better suited to the potential saline conditions of semi-hydroponic environments.

4.3 | Photoperiod Effect

Univariate analysis revealed that several metabolite classes, including amino acids, phenolic compounds, organic acids, and sugars, were significantly influenced by photoperiod (Table 2). This indicates that light and dark phases modulate key aspects of yerba mate's metabolic profile. Among these, sugars such as maltose (C123) and glucose (C121), phenylalanine (C148) and *cis*-caffeic acid (C86), the last two involved in the phenylpropanoid pathway, have been associated with circadian rhythms (Harmer et al. 2000) and also here show a clear photoperiod-dependent variation in yerba mate.

Maltose (C123) and glucose (C121) are key products of starch breakdown, with maltose serving as the primary form of carbon export from chloroplasts during the night (Lu et al. 2005; Lu and Sharkey 2006). In the high-resolution sampling (HRS), maltose levels were photoperiod-dependent: they increased after sunset, peaked around midnight, and declined toward dawn, reaching their lowest levels at midday (Figure 5A). This pattern suggests that maltose metabolism in *yerba mate* is under circadian control and operates independently of clone identity (Lu et al. 2005). In *Arabidopsis*, starch exhibits a pronounced circadian rhythm, accumulating during the day and degrading at night to prevent predawn carbon starvation, as reflected by the nocturnal increase in maltose (C123) in *yerba mate* (Table 2, Figure 5A; Graf et al. 2010; Müller et al. 2014; Venkat and Muneer 2022). This accumulation aligns with the hydrolytic pathway of starch degradation being predominant in leaf metabolism, as also observed in potato leaves (Urbanczyk-Wochniak et al. 2005).

Glucose (C121) showed a significant interaction between photoperiod and clone in the RM-ASCA+ analysis (Figure 4C,F), with elevated levels in clone EC21 during the light period. However, in the HRS dataset, glucose remained relatively stable across all time points. In contrast, maltose (C123) and fructose (C118) were more abundant at night, with maltose reaching its lowest levels at midday and fructose peaking after sunrise (Figure 5A). While most sugars exhibited clone-dependent variation, with EC21 accumulating higher amounts (Table 2), fructose and glucose stood out for their strong photoperiod influence. These sugars are central to carbon and energy metabolism and reflect a light-dependent dynamic (Zheng et al. 2025). Metabolomic profiling revealed synchronized diurnal oscillations of metabolites, indicating circadian regulation of carbon and energy metabolism. This pattern is consistent with distinct diurnal carbon partitioning strategies observed in *Arabidopsis*, potato, and barley (Urbanczyk-Wochniak et al. 2005; Müller et al. 2014; Dantas et al. 2023). Elevated nocturnal sugar levels may represent species-specific adaptations to maintain energy balance throughout the night.

In plants, sucrose is the primary product of photosynthesis and the main transport sugar, showing a strong correlation with trehalose-6-phosphate (Tre6P) across various tissues, developmental stages, and environmental conditions (Lunn et al. 2014). In this study, sucrose (C135) exhibited clone-dependent variation, with higher levels in EC21, potentially reflecting its osmoprotectant role under saline stress (Table 1, Figure 4D; Mehta and Vyas 2023).

Under the high-resolution sampling (HRS) strategy, sucrose showed an interaction effect: clone EC24 maintained relatively stable levels throughout the photoperiod, similar to glucose (Figure 5A), whereas EC21 displayed a distinct peak at midnight (MM) followed by a sharp decline before sunset (BSS) (Figure 5C). This drop in sucrose may be accompanied by a decrease in Tre6P (though typically not detectable by GC–MS) which could facilitate accelerated starch degradation to meet sucrose demand. This pattern aligns with maltose accumulation at night (Figure 5A) and may reflect the regulatory role of Tre6P in balancing sucrose and starch metabolism during the dark phase, linking carbon availability to growth (Lunn et al. 2014; Fichtner et al. 2020). In *yerba mate*, the elevated accumulation of soluble sugars in EC21 may therefore reflect both osmotic adjustment under salt stress and differences in circadian carbon partitioning between semi-hydroponically grown clones.

Caffeoyl-quinic acids are among the most important bioactive compounds in *yerba mate*, contributing significantly to its antioxidant capacity (Heck and De Mejia 2007). These secondary metabolites are synthesized via the phenylpropanoid pathway, with phenylalanine and caffeic acid as key precursors (Clifford et al. 2017). Both compounds tend to accumulate during the light period, consistent with their activation under sunlight and the light-dependent synthesis of phenolics via the phenylpropanoid pathway (Clifford et al. 2017). Interestingly, RM-ASCA+ analysis revealed an interaction effect for phenylalanine, with elevated levels during the dark phase in clone EC24 (Figure 4C,F). However, HRS data showed a photoperiod and interaction effects: phenylalanine peaked from midday to shortly after sunset and declined toward midnight and sunrise, a pattern also observed in potato leaves (Figure 5B; Urbanczyk-Wochniak et al. 2005).

The sum of caffeoyl-quinic acids also showed an interaction effect, yet their temporal profile followed a photoperiod pattern during HRS data: the relative abundances peaked around midnight and remained elevated until sunrise, with the lowest levels observed after sunset (Figure 5B). This contrasting behavior between phenylalanine and its downstream products may

reflect their roles as precursor and end-product within the same biosynthetic pathway (Clifford et al. 2017). Considering chlorogenate as the major soluble phenylpropanoid, its levels increase in potato leaves during the dark period (Urbanczyk-Wochniak et al. 2005). Moreover, the decline in caffeoyl-quinic acids during light conditions may indicate their active consumption to mitigate photooxidative stress. Acting as potent antioxidants, these compounds help protect plant tissues from damage caused by solar radiation, particularly ultraviolet light (Moyo et al. 2022).

Given that both compounds showed interaction effects during HRS, a correlation analysis was performed between phenylalanine and the sum of caffeoyl-quinic acids. Interestingly, only clone EC24 exhibited a significant relationship, modeled by a second-order curve (Figure 5F), in which high levels of caffeoylquinic acids coincided with low levels of phenylalanine. As previously suggested, this pattern reinforces the idea that clone EC24 may possess a more pronounced stress-response mechanism, likely centered on antioxidant pathways (as seen for saline stress), an interpretation further supported by the observed correlation.

4.4 | Nitrogen Metabolism: The Metabolic Plasticity of Clones

Univariate statistical analysis highlighted several nitrogen-containing compounds, caffeine (C156), ornithine (C137), and the TCA cycle intermediate 2-oxo-glutaric acid (C7), as key metabolites showing interaction effects between clone and photoperiod (Table 3). These compounds are involved in nitrogen assimilation, cellular stress responses, and plant defense mechanisms (Buezo et al. 2025; Kim and Sano 2008; Nunes-Nesi et al. 2010). Notably, 2-oxo-glutaric acid (C7) deviates from the general interaction pattern, showing consistently higher levels during the light period in EC24, while EC21 maintains elevated amounts in both dark and light phases (Table 3). As a central intermediate in the TCA cycle, 2-oxo-glutaric acid serves as a direct precursor for the synthesis of several amino acids, particularly through the interconversion of glutamate, a key molecule in nitrogen assimilation (Chandel 2021).

RM-ASCA+ analysis further supports this nitrogen-related dynamic as a metabolomic system as a whole, revealing that amino acids such as glutamine (C145), arginine (C135), asparagine (C139), and alanine (C136), along with citric acid (C129), are associated with the dark period in EC21 and the light period in EC24 (Figure 4C,F). Ornithine (C137) accumulates predominantly during the dark phase in EC21, while its levels remain stable across both photoperiods in EC24 (Table 3). As part of the urea cycle, ornithine plays a crucial role in managing excess ammonium, which may be linked to saline stress and the accumulation of nitrogen cycle intermediates such as glutamine, arginine, and ornithine (Buezo et al. 2025).

Caffeine (C156), a well-known bioactive compound in yerba mate, is notable not only for its physiological effects but also for its heritability (Cardozo Junior et al. 2010; Heck and De Mejia 2007), making it a valuable trait in breeding programs. In EC24, caffeine relative abundance is higher during daylight hours when compared to EC21 daylight, both clones have equal levels at night. Any difference of dark and light periods was detected for EC24, in contrast, EC21 exhibits its highest caffeine levels during the night (Table 3). Yerba mate genotypes can be classified based on caffeine content (de Aguiar et al. 2023; de Tomasi et al. 2024b), and RM-ASCA+ analysis confirms a clone effect, with caffeine (C156) correlating strongly with EC24 (Figure 4A,D). However, the distinct daytime and nighttime distribution of caffeine in EC21 is particularly intriguing. High-resolution sampling (HRS) reveals an interaction between clone and photoperiod: EC24 shows elevated caffeine levels at BSS, BSR, and ASR, while EC21 peaks at MN (Figure 5D). For EC24, the highest amount occurs at BSS, with significantly lower levels at night and early morning (i.e., MN, BSR, and ASR). In EC21, caffeine peaks at MN, showing no significant differences from MM but differing from BSR and ASR.

The statistical evidence supports the view that the interaction reflects a distributed pattern involving multiple metabolites of the nitrogen cycle dynamics, whose combined behavior differentiates clones across photoperiods, making caffeine catabolism a relevant area of investigation. Caffeine degradation involves intermediates such as allantoin, which was also annotated in this study and displays a similar temporal pattern to caffeine in EC21 with higher amounts at MN (Figure 5E). Allantoin (C81) is a key intermediate in purine catabolism, facilitating nitrogen recycling from degraded purines and serving as a significant nitrogen storage and transport molecule, particularly in tropical legumes (Kaur et al. 2023). Elevated levels of caffeine (C156) and allantoin (C81) may contribute to maintaining nitrogen homeostasis and supporting growth during the night by balancing carbon and nitrogen metabolism in the clone EC21. This relationship is supported by a positive correlation between the two compounds in EC21, where a linear regression curve was fitted (Figure 5F). In contrast, no significant correlation was observed in EC24, further highlighting the distinct metabolic strategies employed by each clone.

The contrasting multivariate reorganization of the metabolome between clones suggests that EC24 activates nitrogen metabolism in response to light, while EC21 also relies on nocturnal nitrogen turnover, reflecting distinct strategies of metabolic plasticity. This clone-specific temporal regulation of nitrogen-related compounds underscores the importance of genotype selection in optimizing yerba mate performance under semi-hydroponic and circadian-influenced conditions. Notably, the strategy employed by EC21 appears particularly well-suited to semi-hydroponic cultivation, where the accumulation of nitrogen-related metabolites during the night period may sufficiently support growth demands during the phase (Figure 4F).

5 | Conclusion

This study demonstrates the value of integrating multivariate and univariate approaches to unravel the metabolomic dynamics of yerba mate under semi-hydroponic conditions. High-resolution sampling (HRS) provides a comprehensive view of temporal metabolic shifts, although the complexity of the data can limit interpretation without summarizing specific metabolic patterns. In contrast, targeted comparisons between light

and dark phases prove more effective for independently visualizing metabolite behavior.

The integration of RM-ASCA+ and univariate statistical analysis yielded overlapping results, reinforcing the robustness of the combined approach. Despite their methodological differences, RM-ASCA+ capturing the multivariate relation across experimental factors and univariate analysis assessing each metabolite independently, the convergence of findings strengthens confidence in the identified metabolic markers across clone, photoperiod (dark vs. light), and interaction effects.

Among these factors, the clone effect emerged as most influential, with metabolite distribution reflecting adaptive responses to saline conditions. Clones EC21 and EC24 appear to engage distinct strategies, suggesting metabolic specialization under stress.

The photoperiod effect revealed strategic adaptations to maintain energy balance during the night. Carbohydrates such as fructose, glucose, and maltose accumulated rhythmically, pointing to circadian regulation of carbon metabolism. Additionally, photoperiod influenced the phenylpropanoid pathway, with phenylalanine and caffeic acid contributing to the biosynthesis of caffeoyl-quinic acids, key bioactive compounds in yerba mate.

The interaction factor between clone and photoperiod underscored the metabolic plasticity of yerba mate genotypes. Metabolites involved in nitrogen assimilation, such as glutaric acid, 2-oxo-glutaric acid, glutamine, and ornithine, exhibited clone-specific temporal patterns, reflecting differential regulation of nitrogen metabolism.

Caffeine, a heritable and physiological compound, was associated with clone EC24, particularly during daylight hours. However, EC21 displayed higher caffeine levels at night, a trend confirmed by HRS. This dynamic behavior may be linked to caffeine catabolism, with allantoin, a purine degradation product, showing similar patterns in EC21. These findings suggest that each clone employs distinct strategies for nitrogen turnover and resource allocation, further emphasizing the importance of genotype selection for optimizing yerba mate performance under semi-hydroponic cultivation.

Author Contributions

Tamires O. Melo and **Fabricio A. Hansel:** conceptualization; **Joachim Kopka, Tamires O. Melo, Fabricio A. Hansel:** data curation; **Tamires O. Melo** and **Fabricio A. Hansel:** formal analysis; **Ivar Wendling, Francisco A. Marques** and **Joachim Kopka:** funding acquisition; **Tamires O. Melo, Fabricio A. Hansel** and **Joachim Kopka:** investigation; **Ivar Wendling:** project administration; **Ivar Wendling** and **Joachim Kopka:** resources; **Alexander Erban, Tamires O. Melo** and **Fabricio A. Hansel:** software; **Francisco A. Marques:** supervision; **Tamires O. Melo, Fabricio A. Hansel, Joachim Kopka** and **Ivar Wendling:** validation; **Tamires O. Melo, Alexander Erban, Fabricio A. Hansel, Francisco A. Marques, Joachim Kopka** and **Ivar Wendling:** visualization; **Tamires O. Melo and Fabricio A. Hansel:** Writing – Original Draft Preparation; **Tamires O. Melo, Alexander Erban, Fabricio A. Hansel, Joachim Kopka** and **Ivar Wendling:** Writing – Review and Editing.

Acknowledgments

This study was financed by Embrapa (20.18.01.002.00.03). Tamires O. Melo is grateful to the DAAD-Capes for a scholarship (Edital CAPES no. 15/2017).

Funding

This work was supported by Embrapa Florestas, 20.18.01.002.00.03.

Data Availability Statement

All data supporting the findings of the study are available in https://www.redape.dados.embrapa.br/dataverse/vegetal (https://doi.org/10.48432/8FCY54).

AI Generative Statement

AI assistance was used to refine the manuscript's language for clarity and precision. No content was generated related to data analysis, interpretation, or scientific conclusions.

References

Ashihara, H., H. Sano, and A. Crozier. 2008. "Caffeine and Related Purine Alkaloids: Biosynthesis, Catabolism, Function and Genetic Engineering." *Phytochemistry* 69, no. 4: 841–856. https://doi.org/10.1016/j.phytochem.2007.10.029.

Bertinetto, C., J. Engel, and J. Jansen. 2020. "ANOVA Simultaneous Component Analysis: A Tutorial Review." *Analytica Chimica Acta: X* 6: 100061. https://doi.org/10.1016/j.acax.2020.100061.

Bieniawska, Z., C. Espinoza, A. Schlereth, R. Sulpice, D. K. Hincha, and M. A. Hannah. 2008. "Disruption of the Arabidopsis Circadian Clock Is Responsible for Extensive Variation in the Cold-Responsive Transcriptome." *Plant Physiology* 147, no. 1: 263–279. https://doi.org/10.1104/pp.108.118059.

Bracesco, N. 2019. "*Ilex Paraguariensis* as a Healthy Food Supplement for the Future World." *Biomedical Journal of Scientific & Technical Research* 16, no. 1: 11821–11823. https://doi.org/10.26717/BJSTR.2019.16.002808.

Buezo, J., M. Urra, E. M. González, R. Alcázar, D. Marino, and J. F. Moran. 2025. "The Urea Cycle in Connection to Polyamine Metabolism in Higher Plants: New Perspectives on a Central Pathway." *Physiologia Plantarum* 177, no. 3: e70321. https://doi.org/10.1111/ppl.70321.

Cardozo Junior, E. L., C. M. Donaduzzi, O. Ferrarese-Filho, J. C. Friedrich, A. Gonela, and J. A. Sturion. 2010. "Quantitative Genetic Analysis of Methylxanthines and Phenolic Compounds in Mate Progenies." *Pesquisa Agropecuária Brasileira* 45, no. 2: 171–177. https://doi.org/10.1590/S0100-204X2010000200008.

Chandel, N. S. 2021. "Amino Acid Metabolism." *Cold Spring Harbor Perspectives in Biology* 13, no. 4: a040584. https://doi.org/10.1101/cshperspect.a040584.

Clifford, M. N., I. B. Jaganath, I. A. Ludwig, and A. Crozier. 2017. "Chlorogenic Acids and the Acyl-Quinic Acids: Discovery, Biosynthesis, Bioavailability and Bioactivity." *Natural Product Reports* 34, no. 12: 1391–1421. https://doi.org/10.1039/C7NP00030H.

Dalmagro, A. P., A. Camargo, H. H. da Silva Filho, M. M. Valcanaia, P. C. de Jesus, and A. L. B. Zeni. 2018. "Seasonal Variation in the Antioxidant Phytocompounds Production From the *Morus nigra* Leaves." *Industrial Crops and Products* 123: 323–330. https://doi.org/10.1016/j.indcrop.2018.06.085.

Dantas, L. L., B. M. Eldridge, J. Dorling, D. A. Dekeya, D. A. Lynch, and A. N. Dodd. 2023. "Circadian Regulation of Metabolism Across

Photosynthetic Organisms." *Plant Journal* 116: 650–668. https://doi.org/10.1111/tpj.16405.

de Aguiar, N. S., M. M. Gabira, D. Santin, C. Deschamps, C. V. Helm, and I. Wendling. 2023. "Planting Seasons and Environments in Initial Field Establishment of Yerba Mate Clonal Cultivars in Southern Brazil." *Revista Ceres* 70, no. 6: e70606. https://doi.org/10.1590/0034-737x202370060006.

de Aguiar, N. S., M. Moreno Gabira, J. de Cássia Tomasi, et al. 2022. "Productivity of Clonal *Ilex paraguariensis* Genotypes in a Semi-Hydroponic System Is Reduced by Shading." *Forest Science* 68, no. 5–6: 540–547. https://doi.org/10.1093/forsci/fxac028.

de Tomasi, J. C., N. S. de Aguiar, M. M. Duarte, et al. 2024a. "Bioactive Compound Production in Yerba Mate Clones With Increasing Nitrogen in Semi-Hydroponic System." *Journal of Soil Science and Plant Nutrition* 24, no. 3: 5961–5971. https://doi.org/10.1007/s42729-024-01953-0.

de Tomasi, J. C., N. S. de Aguiar, M. M. Duarte, et al. 2024b. "Nitrogenized Fertigation and Genotype Effects in Yerba Mate Leaf Production in a Semi-Hydroponic System." *Journal of Soil Science and Plant Nutrition* 24, no. 1: 914–921. https://doi.org/10.1007/s42729-023-01595-8.

Dethloff, F., A. Erban, and I. Orf. 2014. "Profiling Methods to Identify Cold-Regulated Primary Metabolites Using Gas Chromatography Coupled to Mass Spectrometry." In *Plant Cold Acclimation: Methods and Protocols*, edited by D. K. Hincha and E. Zuther, 171–197. Springer New York. https://doi.org/10.1007/978-1-4939-0844-8_14.

Dodd, A. N., N. Salathia, A. Hall, et al. 2005. "Plant Circadian Clocks Increase Photosynthesis, Growth, Survival, and Competitive Advantage." *Science* 309, no. 5734: 630–633. https://doi.org/10.1126/science.1115581.

Dong, M. A., and M. F. Farré Thomashow. 2011. "Circadian Clock-Associated 1 and Late Elongated Hypocotyl Regulate Expression of the C-Repeat Binding Factor (CBF) Pathway in Arabidopsis." *Proceedings of the National Academy of Sciences of The United States of America* 108, no. 17: 7241–7246. https://doi.org/10.1073/pnas.1103741108.

Fichtner, F., J. J. Olas, R. Feil, et al. 2020. "Functional Features of Trehalose-6-Phosphate Synthase 1, an Essential Enzyme in *Arabidopsis*." *Plant Cell* 32: 1949–1972. https://doi.org/10.1105/tpc.19.00837.

Fiehn, O. 2002. "Metabolomics – The Link Between Genotypes and Phenotypes." *Plant Molecular Biology* 48, no. 1: 155–171. https://doi.org/10.1023/A:1013713905833.

Filippou, P., X. Zarza, C. Antoniou, et al. 2021. "Systems Biology Reveals Key Tissue-Specific Metabolic and Transcriptional Signatures Involved in the Response of *Medicago truncatula* Plant Genotypes to Salt Stress." *Computational and Structural Biotechnology Journal* 19: 2133–2147. https://doi.org/10.1016/j.csbj.2021.04.018.

Gabira, M. M., Y. Bergeron, M. M. Duarte, et al. 2024. "Morphological, Physiological, and Biochemical Responses of Yerba Mate (*Ilex paraguariensis*) Genotypes to Water Deficit." *New Forests* 55, no. 6: 1771–1785. https://doi.org/10.1007/s11056-024-10059-5.

Gavaghan, C. L., J. V. Li, S. T. Hadfield, et al. 2011. "Application of NMR-Based Metabolomics to the Investigation of Salt Stress in Maize (*Zea mays*)." *Phytochemical Analysis* 22, no. 3: 214–224. https://doi.org/10.1002/pca.1268.

Ghosh, U. K., M. N. Islam, M. N. Siddiqui, and M. A. R. Khan. 2021. "Understanding the Roles of Osmolytes for Acclimatizing Plants to Changing Environment: A Review of Potential Mechanism." *Plant Signaling & Behavior* 16, no. 8: 1913306. https://doi.org/10.1080/15592324.2021.1913306.

Gould, P. D., J. C. W. Locke, C. Larue, et al. 2006. "The Molecular Basis of Temperature Compensation in the Arabidopsis Circadian Clock." *Plant Cell* 18, no. 5: 1177–1187. https://doi.org/10.1105/tpc.105.039990.

Graf, A., A. Schlereth, M. Stitt, and A. M. Smith. 2010. "Circadian Control of Carbohydrate Availability for Growth in *Arabidopsis* Plants at Night." *Proceedings of the National Academy of Sciences of the United States of America* 107, no. 20: 9458–9463. https://doi.org/10.1073/pnas.0914299107.

Gutiérrez, R. A., T. L. Stokes, K. Thum, et al. 2008. "Systems Approach Identifies an Organic Nitrogen-Responsive Gene Network That Is Regulated by the Master Clock Control Gene CCA1." *Proceedings of the National Academy of Sciences of the United States of America* 105, no. 12: 4939–4944. https://doi.org/10.1073/pnas.0800211105.

Harmer, S. L., J. B. Hogenesch, M. Straume, et al. 2000. "Orchestrated Transcription of Key Pathways in Arabidopsis by the Circadian Clock." *Science* 290, no. 5499: 2110–2113. https://doi.org/10.1126/science.290.5499.2110.

Heck, C. I., and E. G. De Mejia. 2007. "Yerba Mate Tea (*Ilex paraguariensis*): A Comprehensive Review on Chemistry, Health Implications, and Technological Considerations." *Journal of Food Science* 72, no. 9: R138–R151. https://doi.org/10.1111/j.1750-3841.2007.00535.x.

Hualpa-Ramirez, E., E. C. Carrasco-Lozano, J. Madrid-Espinoza, et al. 2024. "Stress Salinity in Plants: New Strategies to Cope With in the Foreseeable Scenario." *Plant Physiology and Biochemistry* 208: 108507. https://doi.org/10.1016/j.plaphy.2024.108507.

Hummel, J., N. Strehmel, J. Selbig, D. Walther, and J. Kopka. 2010. "Decision Tree Supported Substructure Prediction of Metabolites From GC-MS Profiles." *Metabolomics* 6, no. 2: 322–333. https://doi.org/10.1007/s11306-010-0198-7.

Husson, F., J. Josse, S. Lê, and J. Mazet. 2014. "FactoMineR: Multivariate Exploratory Data Analysis and Data Mining With R. FactoMineR: Multivariate Exploratory Data Analysis and Data Mining With R.R Package Version." 1: 102–123.

Husson, F., J.Josse, and J. Pagès. 2010. "Principal Component Methods - Hierarchical Clustering - Partitional Clustering: Why Would We Need to Choose for Visualizing Data?." http://factominer.free.fr/more/HCPC_husson_josse.pdf.

Ishitani, M., A. L. Majumder, A. Bornhouser, C. B. Michalowski, R. G. Jensen, and H. J. Bohnert. 1996. "Coordinate Transcriptional Induction of Myo-Inositol Metabolism During Environmental Stress." *Plant Journal* 9, no. 4: 537–548. https://doi.org/10.1046/j.1365-313X.1996.09040537.x.

Jarmund, A. H., T. S. Madssen, and G. F. Giskeødegård. 2022. "ALASCA: An R Package for Longitudinal and Cross-Sectional Analysis of Multivariate Data by ASCA-Based Methods." *Frontiers in Molecular Biosciences* 9: 962431. https://doi.org/10.3389/fmolb.2022.962431.

Johnson, C. H. 2005. "Testing the Adaptive Value of Circadian Systems." In *Methods in Enzymology*, edited by M. W. Young, vol. 393, 818–837. Academic Press. https://doi.org/10.1016/S0076-6879(05)93043-7.

Jolliffe, I. T. 2002. *Principal Component Analysis*, 488. Springer New York, NY. https://doi.org/10.1007/b98835.

Jorge, T. F., N. Duro, M. da Costa, et al. 2017. "GC-TOF-MS Analysis Reveals Salt Stress-Responsive Primary Metabolites in *Casuarina glauca* Tissues." *Metabolomics* 13, no. 8: 95. https://doi.org/10.1007/s11306-017-1234-7.

Kaur, R., J. Chandra, B. Varghese, and S. Keshavkant. 2023. "Allantoin: A Potential Compound for the Mitigation of Adverse Effects of Abiotic Stresses in Plants." *Plants* 12: 3059. https://doi.org/10.3390/plants12173059.

Kiełbowicz-Matuk, A., and J. Czarnecka. 2014. "Chapter 20 - Interplays of Plant Circadian Clock and Abiotic Stress Response Networks." In *Emerging Technologies and Management of Crop Stress Tolerance*, edited by P. Ahmad and S. Rasool, 487–506. Academic Press. https://doi.org/10.1016/B978-0-12-800876-8.00020-5.

Kim, Y.-S., and H. Sano. 2008. "Pathogen Resistance of Transgenic Tobacco Plants Producing Caffeine." *Phytochemistry* 69, no. 4: 882–888. https://doi.org/10.1016/j.phytochem.2007.10.021.

Kopka, J., N. Schauer, S. Krueger, et al. 2005. "GMD@CSB.DB: The Golm Metabolome Database." *Bioinformatics* 21, no. 8: 1635–1638. https://doi.org/10.1093/bioinformatics/bti236.

Kuhlman, S. J., S. R. Mackey, and J. F. Duffy. 2007. "Biological Rhythms Workshop I: Introduction to Chronobiology." *Cold Spring Harbor Symposia on Quantitative Biology* 72, no. 1: 1–6. https://doi.org/10.1101/sqb.2007.72.059.

Lê, S., J. Josse, and F. Husson. 2008. "FactoMineR: An R Package for Multivariate Analysis." *Journal of Statistical Software* 25, no. 1: 1–18.

Lu, Y., J. P. Gehan, and T. D. Sharkey. 2005. "Daylength and Circadian Effects on Starch Degradation and Maltose Metabolism." *Plant Physiology* 138, no. 4: 2280–2291. https://doi.org/10.1104/pp.105.061903.

Lu, Y. A. N., and T. D. Sharkey. 2006. "The Importance of Maltose in Transitory Starch Breakdown." *Plant, Cell & Environment* 29, no. 3: 353–366. https://doi.org/10.1111/j.1365-3040.2005.01480.x.

Luedemann, A., K. Strassburg, A. Erban, and J. Kopka. 2008. "TagFinder for the Quantitative Analysis of Gas Chromatography—Mass Spectrometry (GC-MS)-based Metabolite Profiling Experiments." *Bioinformatics* 24, no. 5: 732–737. https://doi.org/10.1093/bioinformatics/btn023.

Lunn, J. E., I. Delorge, C. M. Figueroa, P. Van Dijck, and M. Stitt. 2014. "Trehalose Metabolism in Plants." *Plant Journal* 79, no. 4: 544–567. https://doi.org/10.1111/tpj.12509.

Madssen, T. S., G. F. Giskeødegård, A. K. Smilde, and J. A. Westerhuis. 2021. "Repeated Measures ASCA+ for Analysis of Longitudinal Intervention Studies With Multivariate Outcome Data." *PLoS Computational Biology* 17, no. 11: e1009585. https://doi.org/10.1371/journal.pcbi.1009585.

Maugeri, A., M. Barchitta, G. Basile, and A. Agodi. 2021. "Applying a Hierarchical Clustering on Principal Components Approach to Identify Different Patterns of the SARS-CoV-2 Epidemic Across Italian Regions." *Scientific Reports* 11: 7082. https://doi.org/10.1038/s41598-021-86703-3.

McClung, C. R. 2006. "Plant Circadian Rhythms." *Plant Cell* 18, no. 4: 792–803. https://doi.org/10.1105/tpc.106.040980.

Mehmood, H., G. H. Abbasi, M. Jamil, Z. Malik, M. Ali, and R. Iqbal. 2021. "Assessing the Potential of Exogenous Caffeic Acid Application in Boosting Wheat (*Triticum aestivum* L.) Crop Productivity Under Salt Stress." *PLoS One* 16, no. 11: e0259222. https://doi.org/10.1371/journal.pone.0259222.

Mehta, D., and S. Vyas. 2023. "Comparative Bio-Accumulation of Osmoprotectants in Saline Stress Tolerating Plants: A Review." *Plant Stress* 9: 100177. https://doi.org/10.1016/j.stress.2023.100177.

Melo, T. O., L. Franciscon, G. Brown, et al. 2021. "Univariate Statistical Analysis of Gas Chromatography – Mass Spectrometry Fingerprints Analyses." *Chemical Data Collections* 33: 100719. https://doi.org/10.1016/j.cdc.2021.100719.

Menegolla, F., F. A. Hansel, J. Degenhardt, and M. Lazzarotto. 2025. "Mini-Cutting Condition on the Identification of Rooting-Biomarkers in Easy- and Hard-To-Root *Ilex paraguariensis* Clones." *Planta* 261, no. 2: 24. https://doi.org/10.1007/s00425-024-04604-x.

Michaeli, S., and H. Fromm. 2015. "Closing the Loop on the GABA Shunt in Plants: Are GABA Metabolism and Signaling Entwined?" *Frontiers in Plant Science* 6: 419. https://doi.org/10.3389/fpls.2015.00419.

Moyo, B., N. T. Tavengwa, and N. E. Madala. 2022. "Diverse Chemical Modifications of the Chlorogenic Acid Composition of Viscum Combreticola Engl.: A Premise for the State of Readiness Against Excessive Sunlight Exposure." *Journal of Photochemistry and Photobiology B: Biology* 233: 112501. https://doi.org/10.1016/j.jphotobiol.2022.112501.

Müller, L. M., M. von Korff, and S. J. Davis. 2014. "Connections Between Circadian Clocks and Carbon Metabolism Reveal Species-Specific Effects on Growth Control." *Journal of Experimental Botany* 65, no. 10: 2915–2923. https://doi.org/10.1093/jxb/eru120.

Nunes-Nesi, A., A. R. Fernie, and M. Stitt. 2010. "Metabolic and Signaling Aspects Underpinning the Regulation of Plant Carbon Nitrogen Interactions." *Molecular Plant* 3, no. 6: 973–996. https://doi.org/10.1093/mp/ssq049.

Palavicini, S. M. S., B. M. S. Puton, R. A. Jacques et al. 2025. "Bioactive Compounds of Ilex Paraguariensis: A Critical Update on Extraction, Gastrointestinal Stability, and Technological Applications." *Journal of Food Science* 90, no. 11: e70679. https://doi.org/10.1111/1750-3841.70679.

Patel, M. K., M. Kumar, W. Li, et al. 2020. "Enhancing Salt Tolerance of Plants: From Metabolic Reprogramming to Exogenous Chemical Treatments and Molecular Approaches." *Cells* 9, no. 11: 2492. https://doi.org/10.3390/cells9112492.

Paul, A., and P. de Boves Harrington. 2021. "Chemometric Applications in Metabolomic Studies Using Chromatography-Mass Spectrometry." *TrAC Trends in Analytical Chemistry* 135: 116165. https://doi.org/10.1016/j.trac.2020.116165.

R CoreTeam. 2018. *A Language and Environment for Statistical Computing*. R Foundation for Statistical Computing. https://www.R-Project.Org.

Richter, J. A., A. Erban, J. Kopka, and C. Zörb. 2015. "Metabolic Contribution to Salt Stress in Two Maize Hybrids With Contrasting Resistance." *Plant Science* 233: 107–115. https://doi.org/10.1016/j.plantsci.2015.01.006.

Salam, U., S. Ullah, Z.-H. Tang, et al. 2023. "Plant Metabolomics: An Overview of the Role of Primary and Secondary Metabolites Against Different Environmental Stress Factors." *Life* 13, no. 3: 706. https://doi.org/10.3390/life13030706.

Santin, D., E. L. Benedetti, N. F. de Barros, et al. 2019. "Adubação nitrogenada e intervalos de colheita na produtividade e nutrição da erva-mate e em frações de carbono e nitrogênio do solo." *Ciência Florestal* 29, no. 3: 1199–1214. https://doi.org/10.5902/1980509810843.

Sengupta, S., S. Mukherjee, P. Basak, and A. L. Majumder. 2015. "Significance of Galactinol and Raffinose Family Oligosaccharide Synthesis in Plants." *Frontiers in Plant Science* 135: 20116165. https://doi.org/10.3389/fpls.2015.00656.

Skoog, D. A., D. M. West, and F. J. Holler. 1996. *Fundamentals of Analytical Chemistry*. 7th ed, 870. Saunders College.

Smilde, A. K., M. E. Timmerman, M. M. W. B. Hendriks, J. J. Jansen, and H. C. J. Hoefsloot. 2012. "Generic Framework for High- Dimensional Fixed-Effects ANOVA." *Briefings in Bioinformatics* 13, no. 5: 524–535. https://doi.org/10.1093/bib/bbr071.

Strehmel, N., J. Hummel, A. Erban, K. Strassburg, and J. Kopka. 2008. "Retention Index Thresholds for Compound Matching in GC–MS Metabolite Profiling." *Journal of Chromatography B* 871, no. 2: 182–190. https://doi.org/10.1016/j.jchromb.2008.04.042.

Sturion, J. A. 2009. Programa de Melhoramento Genético da Erva-Mate Conduzido pela Embrapa Florestas: Situação Atual e Perspectivas Futuras. https://www.infoteca.cnptia.embrapa.br/infoteca/bitstream/doc/657566/1/Doc179.pdf.

Takabe, T. 2012. "Engineering of Betaine Biosynthesis and Transport for Abiotic Stress Tolerance in Plants." *Journal of Plant Biochemistry and Biotechnology* 21, no. 1: 58–62. https://doi.org/10.1007/s13562-012-0143-0.

Thiel, M., B. Féraud, and B. Govaerts. 2017. "ASCA+ and APCA+: Extensions of ASCA and APCA in the Analysis of Unbalanced Multifactorial Designs." *Chemometrics* 31: e2895. https://doi.org/10.1002/cem.2895.

Urbanczyk-Wochniak, E., C. Baxter, A. Kolbe, J. Kopka, L. J. Sweetlove, and A. R. Fernie. 2005. "Profiling of Diurnal Patterns of Metabolite and Transcript Abundance in Potato (*Solanum tuberosum*) Leaves." *Planta* 221, no. 6: 891–903. https://doi.org/10.1007/s00425-005-1483-y.

Valluru, R., and W. Van den Ende. 2011. "*Myo*-Inositol and Beyond – Emerging Networks Under Stress." *Plant Science* 181, no. 4: 387–400. https://doi.org/10.1016/j.plantsci.2011.07.009.

Venkat, A., and S. Muneer. 2022. "Circadian Regulation of Starch Metabolism and Its Impact on Plant Growth." *Frontiers in Plant Science* 13: 836244. https://doi.org/10.3389/fpls.2022.836244.

Vieira, L. M., R. d. A. Maggioni, J. d. C. Tomasi, et al. 2021. "Vegetative Propagation, Chemical Composition and Antioxidant Activity of Yerba Mate Genotypes." *Plant Genetic Resources: Characterization and Utilization* 19, no. 2: 112–121. https://doi.org/10.1017/S1479262121000150.

Wendling, I., L. F. Dutra, and F. Grossi. 2007. "Produção e sobrevivência de miniestacas e minicepas de erva-mate cultivadas em sistema semi-hidropônico." *Pesquisa Agropecuária Brasileira* 42, no. 2: 289–292. https://doi.org/10.1590/S0100-204X2007000200019.

Westphalen, D. J., A. C. Angelo, Ü. B. Rossa, I. A. Bognola, and C. E. N. Martins. 2020. "Impact of Different Silvicultural Techniques on the Productive Efficiency of *Ilex paraguariensis* A.St. Hill. *Agroforestry Systems*." 94, no. 3: 791–798. https://doi.org/10.1007/s10457-019-00451-y.

Zheng, K., M. d. P. Martinez, M. Bouzid, M. Balparda, M. Schwarzländer, and V. G. Maurino. 2025. "Regulation of Plant Glycolysis and the Tricarboxylic Acid Cycle by Posttranslational Modifications." *Plant Journal* 122, no. 1: e70142. https://doi.org/10.1111/tpj.70142.

Supporting Information

Additional supporting information can be found online in the Supporting Information section. **Table S1:** Annotated metabolite codes used in multivariate and univariate analyses. **Figure S1:** Semi-hydroponic system at Embrapa Florestas (Colombo, Paraná, Brazil). Mini-stumps were cultivated in a sand-based semi-hydroponic system under greenhouse conditions, with an average temperature of 25.3°C and no control of relative humidity. Plants were spaced at 15 cm × 15 cm, totaling a density of 44 mini-stumps per square meter. Nutrient solution (pH 5.5; electrical conductivity 2.47 mS cm^{-1}) was delivered via drip fertigation three times daily, totaling 5 mm day^{-1}, and contained: NO_3^- (156.0 mg L^{-1}), NH_4^+ (50.0 mg L^{-1}), P (as PO_4^{2-}, 25.0 mg L^{-1}), K+ (200.0 mg L^{-1}), Ca^{2+} (200.0 mg L^{-1}), Mg^{2+} (45.0 mg L^{-1}), S (as SO_4^{2-}, 76.9 mg L^{-1}), B (as BO_3^{3-}, 1.5 mg L^{-1}), Cu^{2+} (0.1 mg L^{-1}), Fe^{2+} (5.0 mg L^{-1}), Mn^{2+} (1.0 mg L^{-1}), Zn^{2+} (0.7 mg L^{-1}), and Mo^{2-} (0.07 mg L^{-1}). To prevent salt accumulation, the sand substrate was regularly flushed with 40 L of water. **Figure S2:** Bi-plot of principal component analysis (PCA) showing scores and loadings from high-resolution time-point sampling, following $\log_2$ data transformation. Data represent EC24 and EC21 yerba mate clones. Abbreviations: midday (MD), before sunset (BSS), after sunset (ASS), midnight (MN), before sunrise (BSR), and after sunrise (ASR). For metabolite codes in the loading plot, see Table S1, the absence ones indicate unknown metabolites. **Figure S3:** Bi-plot of principal component analysis (PCA) showing scores and loadings from a targeted approach focused exclusively on annotated metabolites (clone × photoperiod: dark/light), following $\log_2$ data transformation. Data represent EC24 and EC21 yerba mate clones. For metabolite codes in the loading plot, see Table S1. **Figure S4:** Hierarchical Clustering on Principal Components (HCPC) based on Ward's criterion, applied to $\log_2$-transformed data from the targeted approach focused exclusively on annotated metabolites (clone × photoperiod: dark/light). Cluster assignment was determined from sample coordinates projected onto the first three principal components. Data represent EC24 (red) and EC21 (blue) yerba mate clones. Abbreviations: midday (MD), before sunset (BSS), after sunset (ASS), midnight (MN), before sunrise (BSR), and after sunrise (ASR). Expected clustering patterns should include separation by clone and/or photoperiod: dark (ASS, MN, BSR) and light (ASR, MD, BSS). Dark periods are indicated by a grey box.